

A Multi-Scale Feature Fusion Framework Integrating Frequency Domain and Cross-View Attention for Dual-View X-ray Security Inspections

Shilong Hong¹, Yanzhou Zhou^{1,2}, Weichao Xu¹✉

¹School of Automation, Guangdong University of Technology, Guangzhou 510006, China

²Guangzhou Institute of Science and Technology, Guangzhou 510006, China
panda@pandacow.cn, {zhouyanzhou, wxu}@gdut.edu.cn

Abstract—With the rapid development of modern transportation systems and the exponential growth of logistics volumes, intelligent X-ray-based security inspection systems play a crucial role in public safety. Although single-view X-ray equipment is widely deployed, it struggles to accurately identify contraband in complex stacking scenarios due to strong viewpoint dependency and inadequate feature representation. To address this, we propose an innovative multi-scale interactive feature fusion framework tailored for dual-view X-ray security inspection image classification. The framework comprises three core modules: the Frequency Domain Interaction Module (FDIM) enhances frequency-domain features through Fourier transform; the Multi-Scale Cross-View Feature Enhancement (MSCFE) leverages cross-view attention mechanisms to strengthen feature interactions; and the Convolutional Attention Fusion Module (CAFM) efficiently fuses features by integrating channel attention with depthwise-separable convolutions. Experimental results demonstrate that our method outperforms existing state-of-the-art approaches across multiple backbone architectures, particularly excelling in complex scenarios with occlusions and object stacking.

Index Terms—Dual-view X-ray inspection, feature fusion, frequency domain, multi-scale, cross-view attention, convolutional attention, X-ray security inspection.

I. INTRODUCTION

As modern transportation systems develop rapidly and logistics volumes grow exponentially, public security faces increasingly severe challenges [1]. In this context, X-ray security inspection systems play a crucial role in detecting prohibited items and ensuring public safety. X-ray inspection equipment is widely used in airports, train stations, customs, post offices, and other public places to examine luggage, parcels, and other items, ensuring they do not contain dangerous goods, contraband, or explosives. However, with the growing complexity of transportation systems, traditional single-view X-ray inspection equipment has become inadequate to meet the increasing security demands.

The widespread use of single-view X-ray inspection equipment has provided basic security guarantees but still faces inherent problems. Due to the limitations of single-view imaging principles, X-rays pass through packages, and materials of varying compositions, densities, and thicknesses absorb X-rays differently, affecting the display of images. Especially in complex stacking scenarios, single-view equipment may

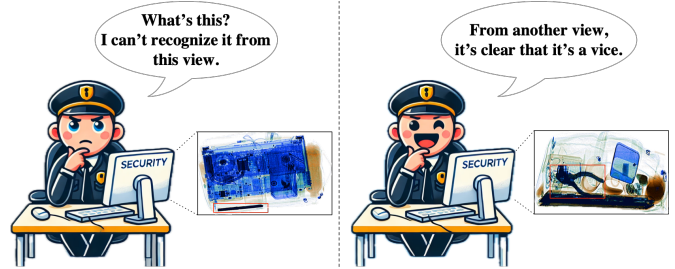


Fig. 1. This image demonstrates the advantages of dual-view, as it reveals features that are not visible in a single view.

not clearly present the complete information of target objects, thereby affecting the detection effectiveness of prohibited items [2–6].

With technological advancements, dual-view X-ray inspection technology has gradually become an important means to address these problems. By simultaneously imaging objects from two orthogonal directions, dual-view X-ray inspection technology significantly enhances the spatial representation of target objects. This is particularly beneficial in complex stacking, angular deviations, and object occlusions, as it can provide more complete contours and morphological information of prohibited items, thereby improving detection accuracy [7]. However, despite significant progress in the practical application of dual-view X-ray equipment, most commercial systems still adopt independent dual-channel detection modes and fail to fully exploit the complementary features between the two views. This results in cross-modal collaborative detection performance far below its theoretical optimum [8]. To address these technical bottlenecks, this paper proposes a multi-scale interactive feature fusion framework for dual-view X-ray security inspection images. The framework comprises three innovative core modules:

- **Frequency Domain Interaction Module (FDIM)**: Extracts frequency-domain features via the Fourier transform and establishes cross-modality feature associations in the frequency domain, effectively enhancing the complementary expression of fine-grained details.
- **Multi-Scale Cross-View Feature Enhancement (MSCFE)**: Employs cross-view attention networks to

✉ Corresponding author.

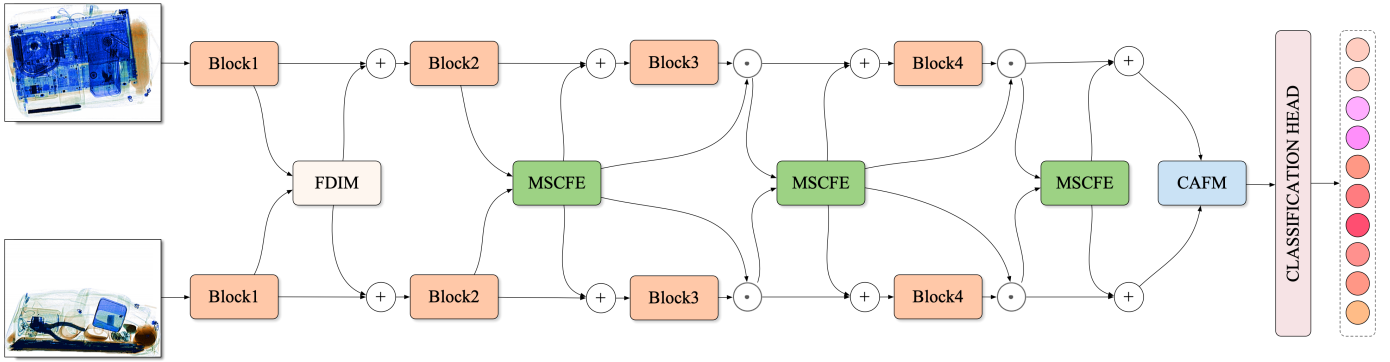


Fig. 2. Overall architecture of the proposed framework.

adaptively strengthen feature interactions between views, improving target discrimination in complex scenarios.

- **Convolutional Attention Fusion Module (CAFM):** Incorporates channel attention mechanisms and depthwise-separable convolution units to precisely fuse dual-view features while suppressing redundancy.

Through systematic experiments on mainstream backbones, ablation studies demonstrate that each module significantly boosts performance. Comparative experiments further show that our model outperforms state-of-the-art methods across multiple backbones.

II. RELATED RESEARCH

In the field of X-ray security image processing, most existing approaches are designed from a single-view perspective, predominantly enhancing feature representations to tackle challenges such as occlusion and complex backgrounds. For instance, the Occlusion-Aware Attention Module (DOAM) [9] focuses on extracting edge information from images, reducing the interference caused by occluded objects by concentrating on their edge features. CFPA-Net [10] employs cross-layer feature fusion (CEF) to reinforce the interaction between high-level semantic features and low-level location cues, thereby improving detection accuracy in complex backgrounds. IEFPN [11] introduces a Layer-based Recalibration Module (LRM) to optimize multi-scale feature fusion on top of a traditional Feature Pyramid Network (FPN), resulting in better detection of targets with varying scales. Methods such as Re-BiFPN [12], and FDTNet [13] have also proposed innovations in feature pyramids, attention mechanisms, and dual-stream networks (combining frequency and spatial domains), respectively, and have seen notable performance gains. However, because these methods are all single-view solutions, they are still constrained by insufficient viewpoint information and struggle with large-angle occlusions or overlapping objects in more complex scenarios.

These methods lay a crucial foundation for subsequent research and collectively improve the performance of prohibited object detection. However, they still face challenges, particularly in effectively using frequency domain and edge information to address occlusion issues.

To further overcome the limitations of single-view methods, researchers have begun exploring dual-view data and networks. With the introduction of dual-view datasets [14], the AHCR [7] approach leverages information exchange between two viewpoints, achieving better detection accuracy in occluded and complex environments. Nevertheless, the existing methodology does not fully exploit the unique characteristics of both dual-view and X-ray security images, leaving room for improvement in situations with extreme occlusions or multiple overlapping items. Some researchers have proposed Transformer-based dual-view methods [15] by refining the attention mechanism for inter-view information exchange. However, these methods exhibit weak generalizability, making them difficult to adapt across various model architectures.

Based on the above analysis, dual-view methods inherently excel at addressing occlusions and overlapping targets, yet the efficient extraction of complementary information between the two viewpoints—particularly leveraging the structural features in X-ray imaging—remains a pressing challenge. In response, we propose a multi-scale interactive feature fusion framework that fully integrates frequency-domain features and attention mechanisms, thereby enhancing feature representation and target recognition accuracy in dual-view X-ray images.

III. METHODOLOGY

A. Overall Architecture

As illustrated in Figure 2, the proposed dual-view X-ray image processing framework is designed to maximize feature extraction efficiency while minimizing computational overhead. We analyze the channel and resolution variations of the backbone network and divide it into four primary modules (some backbones, such as ResNet, may include five modules if a stem layer is counted). Considering the partial similarity between the two views and the need to save computational resources, we employ a weight-sharing backbone structure.

Right after the first module, we introduce the **Frequency Domain Interaction Module (FDIM)**, which extracts frequency-domain features through the Fourier transform and establishes cross-modality feature associations in the frequency domain. This process mainly operates at a relatively higher resolution to enhance fine-grained details.

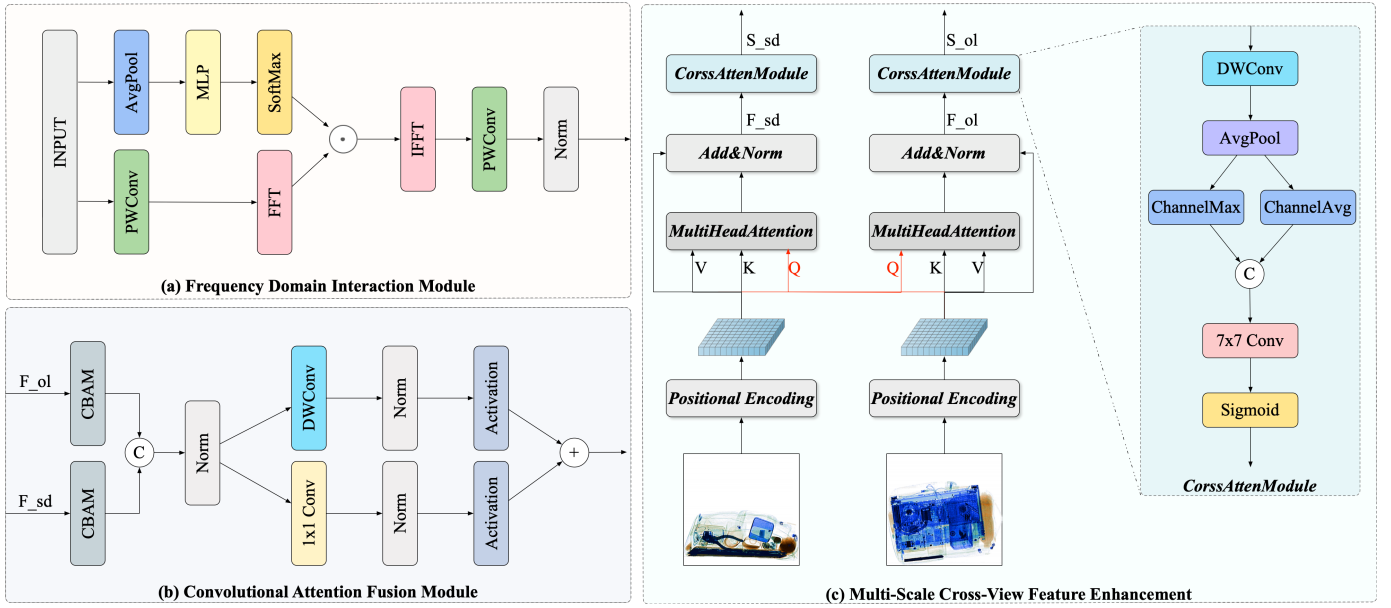


Fig. 3. The sub-modules of the proposed framework: (a) Frequency Domain Interaction Module, (b) Multi-Scale Cross-View Feature Enhancement, (c) Convolutional Attention Fusion Module.

It effectively compensates for the shortcomings of traditional spatial methods in detail capture, thus providing richer feature representations for subsequent fusion and detection.

Subsequently, each of the following modules adopts the **Multi-Scale Cross-View Feature Enhancement (MSCFE)** mechanism to perform feature interaction. In this module, we utilize cross-view attention to enhance feature interactions between different views and introduce adaptive multi-scale feature enhancement to further boost the model's capability in discriminating targets under complex scenarios. The cross-view attention mechanism dynamically adjusts the depth of feature interactions, enabling the model to capture key semantic information at multiple scales while effectively addressing differences in viewpoint.

Finally, we design the **Convolutional Attention Fusion Module (CAFM)** as the last step for refined feature fusion. By leveraging channel attention mechanisms and depthwise-separable convolution units, this module meticulously fuses dual-view features while suppressing redundancy. Through this optimization, the final output has both high discriminative power and avoids superfluous information. With carefully designed module interactions and feature enhancement mechanisms, our framework can maintain computational efficiency while improving the classification performance of dual-view X-ray images. The collaboration among these modules enables the model to provide more accurate detection and classification results, particularly in scenarios with heavily stacked objects and occlusions.

In the following sections, we will detail the design of each module.

B. Frequency Domain Interaction Module (FDIM)

In dual-view X-ray image processing, discrepancies in viewpoints and overlapping objects often lead to feature misalignment and information loss. FDIM is designed to address these challenges by extracting and enhancing features in the frequency domain, leveraging both global (low-frequency) and local (high-frequency) information for more discriminative representations. This approach is inspired by the work of Tsunami et al. [16], who explored the effectiveness of frequency-domain enhancement to mitigate feature misalignment due to viewpoint discrepancies.

1) *Frequency Transform*: As shown in the Figure 3-(a), FDIM first applies Fast Fourier Transform (FFT) [17] to map the input feature maps x and y from the spatial domain into the frequency domain:

$$\tilde{x} = \mathcal{F}(x), \quad \tilde{y} = \mathcal{F}(y) \quad (1)$$

where $\mathcal{F}(\cdot)$ denotes the 2D FFT.

2) *Dynamic Filtering Enhancement*: To enhance discriminative information, FDIM applies dynamic filtering using learnable weight matrices W_x and W_y :

$$\tilde{x}' = \tilde{x} \cdot W_x, \quad \tilde{y}' = \tilde{y} \cdot W_y \quad (2)$$

where W_x and W_y are dynamically computed via an MLP-based weighting mechanism:

$$r_x = P_m(x), \quad r_y = P_m(y) \quad (3)$$

where $P_m(\cdot)$ denote average pooling operations.

$$W_x = \text{Softmax}(\text{MLP}(r_x)) \quad (4)$$

$$W_y = \text{Softmax}(\text{MLP}(r_y)) \quad (5)$$

3) *Inverse Transform and Feature Fusion*: The enhanced frequency-domain features are then transformed back to the spatial domain and fused with the original features using a residual connection:

$$x' = \mathcal{F}^{-1}(\hat{x}') + x \quad (6)$$

$$y' = \mathcal{F}^{-1}(\hat{y}') + y \quad (7)$$

where $\mathcal{F}^{-1}(\cdot)$ denotes the inverse 2D FFT.

This process preserves both spatial contextual information and the fine-grained details extracted in the frequency domain. Compared to methods solely operating in either the spatial or frequency domain, FDIM enables flexible integration of shape and deformation cues across dual-view images, forming a robust foundation for subsequent multi-scale interactions and attention-based fusion.

C. Multi-Scale Cross-View Feature Enhancement (MSCFE)

Due to viewpoint discrepancies and potential object overlaps, dual-view X-ray images (vertical view and horizontal view) often exhibit varying resolutions and complex scenes, posing significant challenges to object recognition. To effectively address these issues, the proposed MSCFE module (Figure 3-(b)) integrates cross-view attention mechanisms with multi-scale information fusion, aiming to balance global and local features while mitigating the effects of occlusions and cluttered backgrounds.

Firstly, the MSCFE module injects positional encoding into the input features of the vertical view branch f_{ol} and the horizontal view branch f_{sd} . Specifically, a 2D sinusoidal positional encoder generates positional embeddings, which are then added to the input features to explicitly embed spatial positional information:

$$F_{ol}^P = F_{ol} + \text{PosEnc}(F_{ol}) \quad (8)$$

$$F_{sd}^P = F_{sd} + \text{PosEnc}(F_{sd}) \quad (9)$$

where F_{ol} denotes the input features from the vertical view branch, F_{sd} denotes the input features from the horizontal view branch, and $\text{PosEnc}(\cdot)$ represents the positional encoding function.

Subsequently, the MSCFE module employs a Multi-Head Cross-Attention mechanism [18–20] to facilitate feature interactions between the vertical and horizontal views. Specifically, the vertical view branch features are used as queries (Query), while the horizontal view branch features serve as keys (Key) and values (Value), and vice versa, enabling bidirectional feature enhancement:

$$F_{sd}^{att} = \text{CrossAttn}(F_{ol}^P, F_{sd}^P) \quad (10)$$

$$F_{ol}^{att} = \text{CrossAttn}(F_{sd}^P, F_{ol}^P) \quad (11)$$

where F_{sd}^{att} and F_{ol}^{att} are the attention-enhanced feature representations for the horizontal and vertical view branches, respectively.

Following the cross-attention operations, the enhanced features are fused with the original input features and subjected to Batch Normalization to maintain feature stability:

$$F_{ol}^E = \text{BatchNorm}(F_{ol}^{att}) + F_{ol} \quad (12)$$

$$F_{sd}^E = \text{BatchNorm}(F_{sd}^{att}) + F_{sd} \quad (13)$$

This approach not only preserves the semantic integrity of the original features but also incorporates useful information discovered through cross-view interactions.

Building upon the fused features, the MSCFE module further refines the representations using Depthwise Separable Convolution (DWConv [21]) to enhance edge and detail representations:

$$F_{ol}^{conv} = \text{DWConv}(F_{ol}^E) \quad (14)$$

$$F_{sd}^{conv} = \text{DWConv}(F_{sd}^E) \quad (15)$$

where F_{ol}^{conv} and F_{sd}^{conv} are the processed features for the vertical and horizontal view branches, respectively.

Additionally, when the module is not the last layer, the MSCFE module introduces optional feature downsampling layers. These layers employ Depthwise Separable Convolutions and pooling operations to construct spatial attention maps. The intermediate pooling results are computed as follows:

$$s_{ol}^{pool} = \text{Concat}(P_m(F_{ol}^{conv}), P_a(F_{ol}^{conv})) \quad (16)$$

$$s_{sd}^{pool} = \text{Concat}(P_m(F_{sd}^{conv}), P_a(F_{sd}^{conv})) \quad (17)$$

where $P_m(\cdot)$ and $P_a(\cdot)$ denote max pooling and average pooling operations.

Next, a 7×7 convolution (denoted as Conv_7) is applied to extract spatial relationships:

$$s_{ol}^{spatial} = \text{Conv}_7(s_{ol}^{pool}) \quad (18)$$

$$s_{sd}^{spatial} = \text{Conv}_7(s_{sd}^{pool}) \quad (19)$$

Finally, activation functions such as Sigmoid are applied to generate the spatial attention maps:

$$s_{ol} = \text{Sigmoid}(s_{ol}^{spatial}) \quad (20)$$

$$s_{sd} = \text{Sigmoid}(s_{sd}^{spatial}) \quad (21)$$

Here, s_{ol} and s_{sd} are the attention maps generated for the vertical and horizontal views, respectively. These attention maps are employed in subsequent layers to weight the features, thereby further enhancing important features and suppressing irrelevant information.

Finally, the MSCFE module outputs the enhanced vertical and horizontal view features along with their corresponding attention maps s_{ol} and s_{sd} . These attention maps are utilized in the following layers to perform weighted feature processing, resulting in more refined and discriminative feature representations.

In summary, the MSCFE module effectively enhances the feature representation capabilities of dual-view (vertical and horizontal) X-ray images by incorporating positional encoding,

multi-head cross-view attention mechanisms, and depthwise separable convolutions. This design significantly improves target recognition accuracy and robustness, especially in complex scenarios involving occlusions and object stacking, while the generated attention maps further optimize subsequent feature processing.

D. Convolutional Attention Fusion Module (CAFM)

After the Frequency Domain Interaction Module (FDIM) and the Multi-Scale Cross-View Feature Enhancement (MSCFE) module incorporate frequency-domain enhancement and cross-view attention, the high-resolution and low-resolution feature maps may still contain redundant or noisy elements. To further refine feature expressiveness while minimizing computational overhead, we introduce the CAFM, as shown in the Figure 3-(c), which combines channel attention mechanisms and depthwise-separable convolutions to achieve efficient and discriminative fusion of dual-view features.

Firstly, the CAFM module applies the Convolutional Block Attention Module (CBAM [22]) to the feature maps from different resolution branches:

$$F'_{ol} = \text{CBAM}(F_{ol}) \quad (22)$$

$$F'_{sd} = \text{CBAM}(F_{sd}) \quad (23)$$

where F'_{ol} and F'_{sd} are the attention-enhanced outputs of the vertical and horizontal view features, respectively. CBAM computes attention weights along both the channel and spatial dimensions, effectively filtering out redundant information while highlighting critical features.

Next, the CAFM module concatenates these attention-refined feature maps along the channel dimension and applies normalization:

$$F_{cat} = \text{concat}(F'_{ol}, F'_{sd}) \quad (24)$$

$$F_{bn} = \text{BatchNorm}(F_{cat}) \quad (25)$$

This fusion ensures the integrity of dual-view information while stabilizing the feature distribution for subsequent convolution operations.

Finally, the CAFM module processes the concatenated and normalized features through a dwcplayer, followed by a ReLU activation function:

$$F_{csp} = \text{dwcplayer}(F_{bn}) \quad (26)$$

$$F_{final} = \text{ReLU}(F_{csp}) \quad (27)$$

where F_{csp} is the feature representation processed by the dwcplayer, and F_{final} is the final output feature map used for classification or detection tasks.

The dwcplayer integrates a single Depthwise Separable Convolution (DWConv) with feature fusion to effectively refine and enhance feature representations while maintaining computational efficiency [23]. ReLU activation effectively suppresses redundant information and retains the most discriminative features.

TABLE I
OVERVIEW OF CURRENT MULTI-VIEW X-RAY DATASETS

Dataset	Positive	Negative	Categories	Availability
DvXray [7]	5,000	11,000	15	Open
MV-Xray [24]	3,231	950	2	No
DBF [25]	2,528	0	4	No

The dwcplayer plays a crucial role within the Convolutional Attention Fusion Module (CAFM). It integrates a single DWConv with feature fusion to effectively enhance and refine feature representations while maintaining computational efficiency. Specifically, the dwcplayer performs the following operations:

Firstly, a 1×1 convolutional layer (**Conv**₁) reduces the channel dimensionality to mitigate computational complexity:

$$F_{x_2} = \text{Conv}_1(F_{bn}) \quad (28)$$

Simultaneously, the input feature is processed via a DWConv to extract spatial features:

$$F_{x_1} = \text{DWConv}(F_{bn}) \quad (29)$$

The outputs of these two feature branches are then element-wise summed to merge information from both pathways:

$$F_{sum} = F_{x_1} + F_{x_2} \quad (30)$$

This design enables dwcplayer to efficiently refine spatial and channel-wise features while preserving essential discriminative information.

The CAFM module effectively fuses dual-view feature maps by combining channel attention mechanisms with a depthwise-separable convolution. The dwcplayer within CAFM ensures that the fused features are refined and enhanced efficiently, preserving important spatial and channel-wise information while suppressing redundant data. This design not only improves the model's accuracy but also ensures computational feasibility during deployment.

IV. EXPERIMENTS

A. Dataset Description

This study utilizes the DvXray [7] dataset provided by Bowen Ma et al., aimed at advancing prohibited item detection in luggage security screening. DvXray is a large-scale dual-view X-ray image dataset comprising 32,000 images, including 5,000 pairs of positive samples and 11,000 pairs of negative samples. The dataset samples are sourced from real subway stations (approximately 66%) and manually designed luggage scanned using X-ray scanners (approximately 34%). It includes 15 categories of common prohibited items, such as firearms, knives, and explosives. All images are in PNG format with a resolution of 800×600 pixels and are annotated at the image level.

As shown in Table I, DvXray is currently the only publicly available dual-view X-ray dataset. Other dual-view datasets are either not publicly released or do not match the scale and category coverage of DvXray. Therefore, DvXray was selected

as the primary data source to ensure the reproducibility and reliability of the experiments.

The dual-view design of the DvXray dataset offers a significant advantage in detecting overlapping items, thereby enhancing the accuracy of prohibited item recognition. The annotation process was carried out by an internal team and verified by professional security personnel to ensure accuracy and reliability. While multi-view images might further improve recognition performance, the dual-view approach strikes an effective balance between computational efficiency and detection effectiveness, meeting the requirements of this study.

B. Experimental Setup

1) *Experimental Environment*: The experiments were conducted on a system equipped with two RTX 4090 GPUs, utilizing CUDA 12.4 and PyTorch 2.5.1 [26]. The dataset was split into training, validation, and test sets with a ratio of 7:2:1. We employed the AdamW optimizer [27] with a total of 60 epochs for training. The batch size was set to 64, and we used 32 workers for data loading to maximize throughput. During training, a warmup strategy was applied, and the learning rate was decayed using the CosineAnnealingLR scheduler [27] to optimize training dynamics.

All models were initialized with ImageNet-1K pre-trained weights to leverage the knowledge learned from the large-scale dataset. Additionally, to enhance training efficiency and model stability, we applied Automatic Mixed Precision (AMP) [28] and Exponential Moving Average (EMA) techniques [29]. These strategies help to accelerate convergence and improve model accuracy by reducing memory usage and smoothing model updates during training.

2) *Loss function*: For the multi-label classification task, we utilized the MultiLabelSoftMarginLoss [26] as the loss function. This function computes the binary cross-entropy loss for each label and averages the losses across all labels. The loss is calculated as follows:

$$L(x, y) = -\frac{1}{C} \sum_{i=1}^C [y_i \cdot \log(\sigma(x_i)) + (1 - y_i) \cdot \log(1 - \sigma(x_i))] \quad (31)$$

where x_i is the predicted value for the i -th label, y_i is the ground truth for the i -th label (taking values 0 or 1), and $\sigma(x_i)$ is the result of applying the Sigmoid activation function to x_i , i.e.,

$$\sigma(x_i) = \frac{1}{1 + \exp(-x_i)} \quad (32)$$

C is the total number of labels. This loss function treats each label as an independent binary classification problem, making it suitable for cases where labels are mutually exclusive.

3) *mAP and AP Calculation*: In multi-label multi-class classification tasks, AP (Average Precision) and mAP (mean Average Precision) are commonly used to evaluate model performance.

TABLE II
COMPARISON OF MODEL PERFORMANCE ACROSS DIFFERENT BACKBONE

Model	FLOPs	Params	Val_mAP	Test_mAP
ResNet50-dual	10.801G	31.929M	0.8093	0.7895
+AHCR	12.405G	34.882M	0.8249	0.8073
+Ours	14.200G	48.302M	0.8533	0.8498
ResNeXt50_32x4d-dual	11.192G	23.041M	0.8696	0.8580
+AHCR	12.808G	34.354M	0.8721	0.8684
+Ours	14.604G	47.774M	0.8754	0.8761
RegNet_x_3.2gf-dual	8.414G	14.318M	0.8291	0.8240
+AHCR	8.717G	16.865M	0.8352	0.8286
+Ours	9.226G	20.089M	0.8389	0.8430
ConvNeXt_Tiny-dual	11.810G	30.194M	0.8823	0.8848
+AHCR	11.887G	29.438M	0.8971	0.8933
+Ours	12.435G	31.381M	0.9151	0.9098

a) *Average Precision (AP)*: AP is calculated for each class by averaging the precision at different recall levels:

$$AP = \frac{1}{n} \sum_{k=1}^n P(k) \cdot \Delta R(k) \quad (33)$$

where $P(k)$ is the precision at the k -th prediction, and $\Delta R(k)$ is the change in recall at that prediction.

b) *Mean Average Precision (mAP)*: mAP is the mean of AP values across all classes:

$$mAP = \frac{1}{C} \sum_{c=1}^C AP_c \quad (34)$$

where C is the total number of classes. mAP gives an overall measure of model performance across all categories.

C. Comparison with Other Methods

To validate the adaptability and effectiveness of the proposed method across different backbone networks, we conducted comparative experiments using ResNet50 [30], ResNeXt50_32x4d [31], RegNet_x_3.2gf [32], and ConvNeXt_Tiny [33] as backbone models. Each backbone was tested with the baseline model (dual), a comparison method (AHCR), and the proposed approach (Ours). The results are presented in Table II.

Overall, the proposed method consistently outperforms both the baseline and AHCR in terms of Val_mAP and Test_mAP across all backbone networks, demonstrating its effectiveness in enhancing dual-view X-ray image classification and its strong generalization capability.

In addition, dual labeling based on the backbone model involves processing the OL and SD views through a shared-weight backbone, concatenating the resulting features, and subsequently passing them through $Conv_1$ before forwarding them to the classification head.

A detailed analysis is as follows:

1. Performance on ResNet50 Compared to the baseline model, the proposed method improves Val_mAP from 0.8093 to 0.8533 and Test_mAP from 0.7895 to 0.8498, significantly

TABLE III
ABLATION STUDY ON DIFFERENT MODEL COMPONENTS

Model	FLOPs	Params	Val_mAP
ResNet50-dual	10.801G	31.929M	0.8093
+CAFM	11.875G	42.979M	0.8252
+MSCFE	12.990G	37.227M	0.8336
+FDIM	12.957G	32.340M	0.8342
+MSCFE & FDIM	15.146G	37.637M	0.8304
+CAFM & MSCFE	14.064G	48.276M	0.8446
+CAFM & FDIM	14.031G	43.389M	0.8334
+ALL	16.220G	48.686M	0.8527

outperforming AHCR (0.8249 and 0.8073, respectively). This indicates that the proposed enhancements effectively exploit dual-view information, yielding substantial improvements even in a conventional CNN architecture.

2. Performance on ResNeXt50_32x4d Leveraging grouped convolutions, this architecture provides stronger feature extraction capabilities, leading to higher classification accuracy across all methods. The proposed approach achieves a Val_mAP of 0.8754, a 0.58% improvement over the baseline and a 0.33% improvement over AHCR, with similar gains observed in Test_mAP. This result suggests that the proposed method can further enhance performance even within more advanced feature extraction frameworks.

3. Performance on RegNet_x_3.2gf Designed for optimized parameter efficiency, this network maintains relatively low computational complexity while delivering competitive classification performance. The proposed method improves Val_mAP from 0.8291 to 0.8389 and Test_mAP from 0.8240 to 0.8430, demonstrating its robustness and adaptability.

4. Performance on ConvNeXt_Tiny Incorporating CNN and Transformer-inspired architectural principles, ConvNeXt provides superior feature representation. The proposed method achieves a Val_mAP of 0.9151, marking a 3.29% increase over the baseline and a 1.80% increase over AHCR, while also achieving a Test_mAP of 0.9098. These results confirm that the proposed enhancements generalize well across networks of varying depths and feature extraction paradigms.

D. Ablation Study Analysis

To evaluate the impact of different functional modules on model performance, we conducted ablation experiments on the DvXray dataset. Previous research has demonstrated the superiority of dual-view imaging over single-view for mitigating object occlusion; therefore, ResNet50-dual was directly adopted as the baseline model. On this basis, various feature enhancement modules were progressively incorporated to investigate their contributions to classification performance. The experimental results are presented in Table III.

For individual module evaluation, CAFM improves the channel-wise feature representation, increasing Val_mAP from 0.8093 to 0.8252. While this confirms its effectiveness in feature fusion, the performance gain remains limited when used alone. MSCFE further enhances feature interactions between dual views, improving cross-view information utilization and

achieving a Val_mAP of 0.8336, representing a 2.99% increase over the baseline. FDIM optimizes feature alignment across views by guiding feature fusion in the frequency domain, leading to a Val_mAP of 0.8342, demonstrating its effectiveness in reducing viewpoint discrepancies.

In module combination experiments, the integration of CAFM and MSCFE further improves Val_mAP to 0.8446, which is 1.1% higher than using MSCFE alone. This indicates that the synergy between channel attention and multi-scale interactive feature extraction enhances feature fusion. The combination of CAFM and FDIM achieves a Val_mAP of 0.8334, slightly lower than FDIM alone, suggesting that channel attention and frequency-domain alignment may introduce redundant information under certain conditions, affecting model convergence. The MSCFE and FDIM combination results in a Val_mAP of 0.8304, lower than their individual performances, which may be attributed to conflicts between multi-scale feature extraction and frequency-domain feature alignment, leading to feature distribution inconsistencies.

When all modules are integrated (+ALL), the model achieves the best performance with a Val_mAP of 0.8527, representing a 5.36% improvement over the baseline. This confirms that each module contributes to different aspects of feature representation and cross-view alignment, and their collaborative optimization further enhances classification performance. However, the results also indicate that the impact of module combinations varies, with MSCFE contributing the most among single modules, whereas FDIM exhibits instability when combined with other modules. Therefore, in practical applications, selecting appropriate module combinations based on specific scenarios and computational constraints is essential to achieving an optimal balance between efficiency and accuracy.

V. CONCLUSION

In this paper, we presented a novel multi-scale interactive feature fusion framework for dual-view X-ray security inspection. Our method enhances feature representation through frequency-domain interactions and multi-scale attention, significantly improving classification accuracy. Experimental results show that our approach consistently outperforms state-of-the-art methods across multiple backbone networks, demonstrating its robustness and adaptability. Future work will focus on further improving feature fusion techniques and exploring real-world applications for security screening.

ACKNOWLEDGMENT

This work was supported in part by a national science foundation, and in part by other supporting funds. The authors would like to express their gratitude to all anonymous reviewers for their valuable comments and suggestions, which have significantly improved the quality of this paper.

REFERENCES

- [1] S. Akcay and T. P. Breckon, "An evaluation of region based object detection strategies within x-ray baggage security imagery," in 2017

- IEEE International Conference on Image Processing (ICIP)*. IEEE, 2017, pp. 1337–1341.
- [2] B. Wang, L. Zhang, L. Wen, X. Liu, and Y. Wu, “Towards real-world prohibited item detection: A large-scale x-ray benchmark,” in *2021 IEEE/CVF International Conference on Computer Vision (ICCV)*, 2021, pp. 5392–5401.
 - [3] C. Zhao, L. Zhu, S. Dou, W. Deng, and L. Wang, “Detecting overlapped objects in x-ray security imagery by a label-aware mechanism,” *IEEE Transactions on Information Forensics and Security*, vol. 17, pp. 998–1009, 2022.
 - [4] S. Akçay, M. E. Kundegorski, C. G. Willcocks, and T. P. Breckon, “Using deep convolutional neural network architectures for object classification and detection within x-ray baggage security imagery,” *IEEE Trans. Inf. Forensics Security*, vol. 13, no. 9, pp. 2203–2215, Sep. 2018.
 - [5] C. Miao and al., “Sixray: A large-scale security inspection x-ray benchmark for prohibited item discovery in overlapping images,” in *Proc. IEEE/CVF Conf. Comput. Vis. Pattern Recognit. (CVPR)*, Jun. 2019, pp. 2119–2128.
 - [6] R. Tao and al., “Towards real-world x-ray security inspection: A high-quality benchmark and lateral inhibition module for prohibited items detection,” in *Proc. IEEE/CVF Int. Conf. Comput. Vis. (ICCV)*, Oct. 2021, pp. 10923–10932.
 - [7] B. Ma, T. Jia, M. Li, S. Wu, H. Wang, and D. Chen, “Towards dual-view x-ray baggage inspection: A large-scale benchmark and adaptive hierarchical cross refinement for prohibited item discovery,” *IEEE Transactions on Information Forensics and Security*, 2024.
 - [8] A. Singh and Dhiraj, “Advancements in machine learning techniques for threat item detection in x-ray images: a comprehensive survey,” *International Journal of Multimedia Information Retrieval*, vol. 13, no. 4, p. 40, 2024.
 - [9] Y. Wei, R. Tao, Z. Wu, Y. Ma, L. Zhang, and X. Liu, “Occluded prohibited items detection: An x-ray security inspection benchmark and de-occlusion attention module,” in *Proceedings of the 28th ACM international conference on multimedia*, 2020, pp. 138–146.
 - [10] Y. Wei, Y. Wang, and H. Song, “Cfpa-net: Cross-layer feature fusion and parallel attention network for detection and classification of prohibited items in x-ray baggage images,” in *2021 IEEE 7th International Conference on Cloud Computing and Intelligent Systems (CCIS)*, 2021, pp. 203–207.
 - [11] J. Liu, X. Liu, F. Qu, H. Zhang, and L. Zhang, “A defect recognition method for low-quality weld image based on consistent multiscale feature mapping,” *IEEE Transactions on Instrumentation and Measurement*, vol. 71, pp. 1–11, 2022.
 - [12] F. Author, S. Author, and T. Author, “Re-bifpn: Refining bifpn for accurate object detection in images,” in *Proceedings of the IEEE Conference on Computer Vision and Pattern Recognition (CVPR)*, 2022, pp. 1234–1245.
 - [13] Z. Zhu, Y. Zhu, H. Wang, N. Wang, J. Ye, and X. Ling, “Fdtnet: Enhancing frequency-aware representation for prohibited object detection from x-ray images via dual-stream transformers,” *Engineering Applications of Artificial Intelligence*, vol. 133, p. 108076, 2024.
 - [14] R. Tao, H. Wang, Y. Guo, H. Chen, L. Zhang, X. Liu, Y. Wei, and Y. Zhao, “Dual-view x-ray detection: Can ai detect prohibited items from dual-view x-ray images like humans?” *arXiv preprint arXiv:2411.18082*, 2024.
 - [15] X. Meng, H. Feng, Y. Ren, H. Zhang, W. Zou, and X. Ouyang, “Transformer-based dual-view x-ray security inspection image analysis,” *Engineering Applications of Artificial Intelligence*, vol. 138, p. 109382, 2024.
 - [16] Y. Tatsunami and M. Taki, “Fft-based dynamic token mixer for vision,” in *Proceedings of the AAAI Conference on Artificial Intelligence*, vol. 38, no. 14, 2024, pp. 15 328–15 336.
 - [17] R. C. Gonzalez and R. E. Woods, *Digital Image Processing*, 4th ed. Pearson, 2018.
 - [18] W. Fang, J. Fan, Y. Zheng, J. Weng, Y. Tai, and J. Li, “Guided real image dehazing using ycber color space,” in *Proceedings of the AAAI Conference on Artificial Intelligence*, 2025, pp. xxxxx–xxxxx.
 - [19] A. Dosovitskiy et al., “Image transformers,” in *Proceedings of the 37th International Conference on Machine Learning (ICML)*, 2020, pp. 298–306.
 - [20] Z. Liu, Y. Lin, Y. Cao, H. Hu, Y. Wei, Z. Zhang, H. Li, B. Guo, and L. Zhang, “Swin transformer: Hierarchical vision transformer using shifted windows,” in *Proceedings of the IEEE International Conference on Computer Vision (ICCV)*, 2021, pp. 10012–10022.
 - [21] A. G. Howard, M. Zhu, B. Chen, D. Kalenichenko, W. Wang, T. Weyand, M. Andreetto, and H. Adam, “Mobilenets: Efficient convolutional neural networks for mobile vision applications,” in *Proceedings of the IEEE Conference on Computer Vision and Pattern Recognition (CVPR)*, 2017, pp. 2285–2294.
 - [22] S. Woo, J. Park, J.-Y. Lee, and I. S. Kweon, “Cbam: Convolutional block attention module,” in *Proceedings of the European Conference on Computer Vision*, 2018, pp. 3–19.
 - [23] C.-Y. Wang, H.-Y. Mark Liao, Y.-H. Wu, P.-Y. Chen, J.-W. Hsieh, and I.-H. Yeh, “Cspnet: A new backbone that can enhance learning capability of cnn,” in *Proceedings of the IEEE/CVF Conference on Computer Vision and Pattern Recognition Workshops*, 2020, pp. 390–391.
 - [24] J.-M. O. Steitz, F. Saeedan, and S. Roth, “Multi-view x-ray r-cnn,” in *German Conference on Pattern Recognition*. Springer, 2018, pp. 153–168.
 - [25] B. K. Isaac-Medina, C. G. Willcocks, and T. P. Breckon, “Multi-view object detection using epipolar constraints within cluttered x-ray security imagery,” in *Proceedings of the 25th International Conference on Pattern Recognition (ICPR)*, 2021, pp. 9889–9896.
 - [26] A. Paszke, S. Gross, S. Chintala, G. Chanan, E. Yang, Z. DeVito, M. Killeen, Y. Lin, A. Nath, A. Lerer et al., “Pytorch: An imperative style, high-performance deep learning library,” *Proceedings of NeurIPS*, vol. 32, 2019.
 - [27] I. Loshchilov and F. Hutter, “Decoupled weight decay regularization,” in *International Conference on Learning Representations (ICLR)*, 2019. [Online]. Available: <https://arxiv.org/abs/1711.05101>
 - [28] P. Micikevicius, S. Narang, G. Alben, G. Diamos, E. Elsen, B. Ginsburg et al., “Mixed precision training,” in *Proceedings of the International Conference on Learning Representations (ICLR)*, 2018.
 - [29] B. T. Polyak and A. Juditsky, “Acceleration of stochastic approximation by averaging,” in *SIAM Journal on Control and Optimization*, vol. 30, no. 4, 1992, pp. 838–855.
 - [30] K. He, X. Zhang, S. Ren, and J. Sun, “Deep residual learning for image recognition,” in *Proceedings of the IEEE/CVF Conference on Computer Vision and Pattern Recognition*, 2016, pp. 770–778.
 - [31] S. Xie, R. Girshick, P. Dollár, Z. Tu, and K. He, “Aggregated residual transformations for deep neural networks,” in *Proceedings of the IEEE Conference on Computer Vision and Pattern Recognition*, 2017, pp. 1492–1500.
 - [32] I. Radosavovic, R. P. Kosaraju, R. Girshick, K. He, and P. Dollár, “Designing network design spaces,” in *Proceedings of the IEEE Conference on Computer Vision and Pattern Recognition*, 2020, pp. 10428–10436.
 - [33] Z. Liu, H. Mao, C.-Y. Wu, C. Feichtenhofer, T. Darrell, and S. Xie, “A convnet for the 2020s,” *arXiv preprint arXiv:2201.03545*, 2022.